Journal of Spacecraft and Rockets

VOLUME 7 APRIL 1970 NUMBER 4

Infrared Moon: A Review

RICHARD W. SHORTHILL
Boeing Scientific Research Laboratories, Seattle, Wash.

Introduction

THE brightness temperature of the lunar surface has been determined using telescopes on Earth, on balloons, and on aircraft. Observations revealed more than a thousand anomalous regions (hot spots) during an eclipse. It was also discovered that certain of the mare and portions of mare regions show an anomalous thermal behavior. In 1966 and 1968 Surveyors I, III, V, VI, and VII performed in situ thermal measurements. With the two Apollo landings in 1969, we have passed from a remote sensing to a physical sampling era. Apollo 11 and 12 provided samples of the lunar surface from which certain of its thermophysical properties will be determined. In the coming Apollo missions, it can be expected that a landing will be made on or at least near one of the so-called hot spots, and on one of the enhanced mare locations.

The purpose of this paper is to describe the infrared measurements that have been made of the lunar surface. The earliest measurement was made one hundred years ago.[1] The first significant work was done between 1924 and 1928 by Pettit and Nicholson of the Mount Wilson Observatory[2]; their work has been reviewed in detail by others.[3-5] They reported measurements of brightness temperatures under various conditions: distribution of temperature along the lunar diameter at full moon, the subsolar point temperatures as a function of phase, the antisolar point (nighttime) temperature and the transient temperature during a total lunar eclipse for a point near the disk center and at the limb. In the theoretical work that followed, Wesselink[6] and Jaeger and Harper[7,8] assumed that the thermophysical properties of the lunar surface were constant with depth and temperature. Even with a two-layer model,[7] it was not possible to match simultaneously the lunation and eclipse measurements with one set of thermal parameters. These early theoretical studies, however, did suggest that the uppermost layer of the moon was of a porous or dustlike nature. Further measurements of eclipse cooling were made by Sinton and Strong in 1953,[9] and in 1958 and 1959 Sinton constructed isothermal contour maps over the lunar surface at nine different phases.[10] The lunar infrared measurements up to 1960, including a description of certain theoretical models, have been discussed by Sinton.[4]

During the lunar eclipse of March 13, 1960, Shorthill, Borough, and Conley[11] discovered that several rayed craters cooled less rapidly than their environs, and in particular, that Tycho was about 40°K warmer than its environs an hour into the umbral phase. This surprising observation in the infrared, revealing differential properties over localized regions, provided an impetus to the author as well as several others to make additional measurements. Subsequently, extensive measurements were made during eclipses and during the lunar daytime. Measurements during the lunar night are less extensive. Some results of these measurements will be discussed as well as a new thermophysical model developed by Winter and Saari[12] which fits both the lunation and eclipse data.

Experimental

Ground-based infrared measurements are complicated by absorption in the Earth's atmosphere. A known temperature source outside the Earth's atmosphere must be used for calibrating, or all the loss factors between the lunar surface and the detector must be determined. The scanning techniques and position determination depend somewhat on the instrumentation.

Richard W. Shorthill is a scientist in the Geo-Astrophysics Laboratory of the Boeing Scientific Research Laboratories. He attended the University of Utah where he earned the B.S. and Ph.D. degrees in Physics in 1954 and 1959. Since starting work at Boeing 10 years ago, he has done extensive research on lunar radiometry and photometry. During the lunar eclipse of March 1960 he discovered the anomalous cooling of ray craters. High resolution isothermal and isophotic mapping of the moon was done throughout a lunation. During the lunar eclipse in December of 1964, using the 73-in. Kottomia telescope in Egypt, more than 1000 lunar hot spots were identified and a series of high resolution isothermal maps were subsequently constructed. He works actively with various NASA centers and government organizations on thermal and photometric properties of the lunar surface. Dr. Shorthill is also a Principal Investigator on the Viking 1975 Mars Mission. He is the author or coauthor of numerous scientific reports, papers, and chapters in several books, and he is a member of AAS, ASP, OSA, RASC, Sigma Xi, Sigma Pi Sigma, and AAAS.

Presented as Paper 69-593 at the AIAA 4th Thermophysics Conference, San Francisco, Calif., June 16-18, 1968; received May 23, 1969; revision received December 15, 1969.

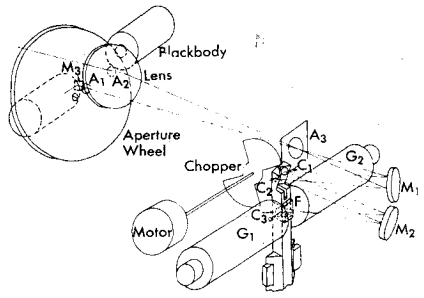

Fig. 1 Diagram of Sinton's pyrometer. A_1 and A_2 are the two defining apertures.[13]

Instruments, Scanning Techniques, and Data Recording

A thermopile was used to obtain the first lunar temperature measurement.[1] Making reasonable assumptions for the moon's albedo and atmospheric losses, Rosse[1] in 1868 determined a brightness temperature of 397°K. Pettit and Nicholson,[2] using extremely fine thermocouples with a rock salt window, determined a brightness temperature of the subsolar point to be 407°K. Using more modern infrared techniques, Sinton[13] developed a "pyrometer" for measuring planetary temperatures. His system (Fig. 1) employs chopping rather than opposing junctions used in the earlier measurements to eliminate drift. It has a tuning fork with reflecting crystal filters C_1, C_2, C_3, and C_4 transmission filter F, and two Golay cells, G_1 and G_2, to look at two separated regions (the sky alone and the moon plus sky) in the focal plane. As the chopper rotates, the images fall alternately on G_1 and G_2, and only the difference in energy between the two regions is amplified. A thermistor bolometer was used by Shorthill to make the first measurements of the anomalous cooling of the ray crater Tycho.[5]

The thermocouple, Golay cell, and thermistor have a relatively slow time response, and measurements were thus limited to a few features, or many hours were required to scan the entire disk. With the development of germanium infrared photodetectors of much greater sensitivity and speed, it became possible to design a system for acquiring measurements over the disk in 15–30 min. Figure 2 shows a cutaway view of the instrument developed by Shorthill and Saari.[14,15] The incoming beam from the Newtonian flat is interrupted by the polished aluminum chopper that reflects the radiation onto the aperture of the detector. Behind the aperture are a series of $f/5.6$ baffles and a 10- to 12-μ filter. A cone channel condenser finally transfers the radiation onto a mercury-doped germanium photodetector which was cooled with liquid hydrogen or neon. The detector used for the simultaneous measurement of the visible radiation was a Dumont 6362 photomultiplier with the same field of view as the infrared photodetector.

A more sensitive infrared bolometer using a gallium-doped single crystal germanium cooled to 2°K was developed by Low[16] and is being used for lunar nighttime measurements by Low and others.

Early measurements were made by moving the telescope to the desired position on the lunar surface by observing a portion of the lunar image adjacent to the defining aperture. Sinton[10] obtained drift curves by moving away from the moon; then the telescope drive was turned off, allowing the moon to drift across the detector, covering a diametral scan and return in 3 min. The motion of the moon in declination resulted in the vertical displacement of subsequent drift scans from which thermal contour maps were constructed. By comparison, a similar scan across the lunar diameter, with the faster Hg-Ge photodetector required 5 sec. In order to employ this rapid scan technique, it was necessary to track the moon by observing a small lunar feature while the infrared detector moved in the focal plane across the lunar image as shown in Fig. 3. The tracking was accomplished with a moderate-sized guide scope. The telescope drive was set near lunar rate, and small differential corrections to the tracking were made during a scanning sequence when necessary. The rapid scan technique was used on the illuminated moon and during an eclipse because surface features were visible. On the dark side, features were not usually visible, so a modified technique was used. A visible feature was located near the terminator, and the telescope either drifted or was driven across the terminator onto the dark side. If the dark limb of the moon can be observed, it aids in the determination of the track across the disk.

Various techniques are now employed for recording, depending on the type of data analyses to be done. Simultaneous chart records, FM magnetic tape recordings, and punched tapes have been used. Salisbury[17] recorded his measurements in the form of reconstructed thermal images. For measurement over the entire disk, the data were recorded on magnetic tape or punched tape and reduced by a high-speed computer. Typically, 200 scan lines over the full moon at 10 arcsec resolution produced 200,000 data points.

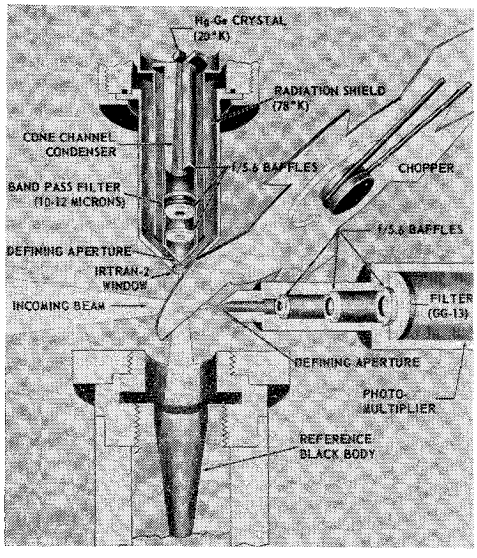

Fig. 2 Cut-away of the instrument used by Shorthill and Saari[14] showing the photomultiplier and mercury-doped germanium detector assemblies, the blackbody reference source and reflecting chopper.

Location Identification

When the telescope and detector are collimated, identification of the region being measured can be accomplished by observing visually or by taking photographs. If the telescope or the detector is moving, it becomes more difficult to relate

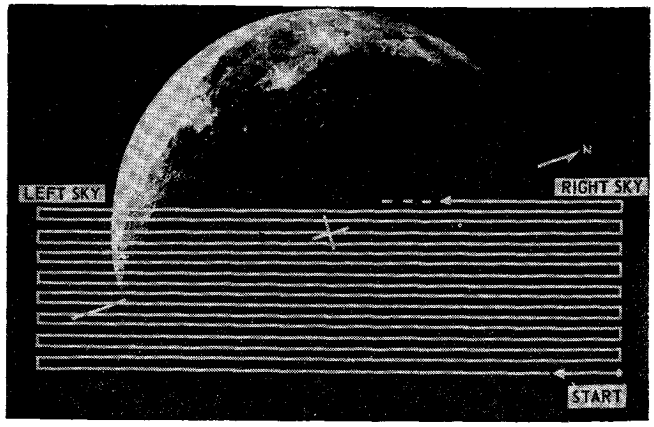

Fig. 3. Rapid scan format. The detector moves over the image in the focal plane (every fifth scan line shown in the figure).

recorded signal variations to given surface features. In principle, if lunar rates, telescope rates, scanning rates, and directions, along with at least one surface feature on the record are known, positions can be determined. Most observers have used the bright and/or terminator signal to orient their maps. Saari and Shorthill used a different method.[15] When the moon was scanned, neither position nor rotation of the raster pattern relative to the moon was accurately known. Infrared and visible radiation were recorded simultaneously, then digitized, and photometric and isothermal contours were constructed for the visible portion of the lunar disk. Small lunar features were identified on the photometric contours by their contrasting albedo, by their shadows, by their corresponding infrared signature and by using photographs taken after each scan program. A transformation was determined by a least-squares fit between the observed scanner coordinates of these small features and an orthographic ξ,η librated grid to correspond to the topocentric position of the moon at the time of the scan. New scanner coordinates were determined for each feature by using the transformation. The rms value of the residuals between observed and calculated position was determined to be a fraction of the resolution element.

Measurements

Lunar daytime

The first survey of lunar daytime temperatures was done with 25-arcsec resolution (1 arcsec corresponds to approximately $\frac{1}{1800}$ of the lunar diameter) by Sinton,[10] who used a narrow-band filter at 8.8 μ and constructed isothermal maps at nine different phases for the illuminated portion of the surface. Saari and Shorthill[15] did a study, using a 10- to 12-μ filter, for 23 phase angles from $-125°$ to $+135°$ (including simultaneous measurements in the visible). With resolutions of 8 and 10 arcsec the isothermal contours could easily be related to surface features. The ξ,η grid lines were drawn for every 0.1 of the lunar radius. Salisbury[17] scanned the lunar disk at several different phases and produced images.

Lunar eclipse

The measurements of Pettit,[18] Sinton,[4] and the survey of a limited number of ray craters during the September 5–6, 1960 eclipse by Saari and Shorthill[19] provided a qualitative indication of the surface cooling. During the eclipse of Dec. 18–19, 1964, however, scans of the entire disk at 10 arcsec resolution were made at four times during the penumbral phase and three times during totality. Both thermal contours and reconstructed thermal images were produced.

Lunar nighttime

The postsunset cooling of the lunar surface is not well determined. Measurements have been made by Shorthill and Saari[14] and Murray and Wildey[20] using a mercury-doped germanium photodetector. The Surveyor spacecraft also made postsunset measurements.[21] Figure 4 shows examples of lunar nighttime cooling. Murray and Wildey[22] made scans over the darkside and produced a thermal contour map of the nighttime portion for the third quarter moon. Postmidnight measurements are especially difficult, requiring very sensitive instrumentation. Low[23] used a germanium bolometer incorporating an interference filter with 17.5 μ wavelength cuton to make repeated scans across the unilluminated moon and reported predawn surface temperatures of approximately 90°K. His survey is continuing.

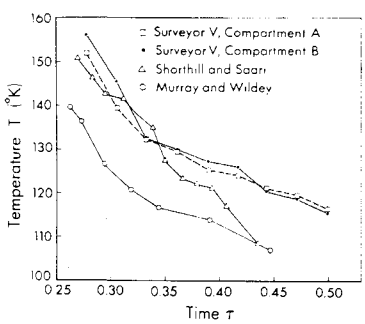

Fig. 4 Lunar nighttime cooling for a region near the lunar equator. τ is fraction of lunation; sunset is at 0.25 τ.

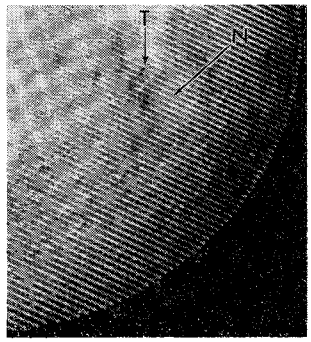

Fig. 5 Infrared image of a full moon scan. The data were obtained at phase of $-2°$ 16′.1 at 23^H $34^M.3$ *UT* on Dec. 18, 1964. The moon was scanned with 200 lines. The every-other-line effect is caused by the electronic enhancing of the image.

Calibration

The absolute calibration of an infrared system through the atmosphere includes a number of difficulties,[24] the most troublesome being the losses in the optical system and in the atmosphere. It is possible to determine the optical losses with an extended blackbody calibration source external to the telescope;[25] however, there are practical difficulties with large telescopes. Determination of atmospheric losses depends upon a knowledge of atmospheric composition (i.e., water vapor), pressure, and temperature with altitude, the zenith angle, and the extinction law as a function of wavelength.

Shorthill and Saari[15] calibrated their data using a calculation of the brightness temperature of the subsolar point when it was visible from the Earth. When the subsolar-point was on the farside, the calibration was accomplished by taking into account atmospheric and optical losses and the night-to-night variations of detector sensitivity.

During the lunar nighttime, calibration is more difficult. Previously measured regions of the illuminated surface could be used for calibrating. Several investigators refer their measurements to other planets for calibration.[22,23] Eclipse calibration for the measurements of Shorthill and Saari[26] was accomplished with respect to the computed subsolar point on the full moon at the start of the eclipse. Sun-moon distance, local surface albedo variations, and directional effects (to be described later) were taken into account. Corrections were made to the extinction coefficient taking into account the precipitable water inferred from ground level humidity measurements.

Observational Results

Daytime Infrared Moon

Under conditions of solar illumination the temperature of the lunar surface is determined by the solar constant, the angle of the sun to the local surface, and the albedo of the surface. With sufficient resolution, the variations caused by local slopes and local albedo can be observed. The northwestern interior slopes of the crater Theophilus (region *T* in Fig. 5, $\xi = 0.435$, $\eta = -0.198$) are cooler (darker in Fig. 5) because at the local surface the elevation angle of the sun is smaller, whereas the southeastern slopes are warmer (brighter) because the local surface is more normal to the sun. Mare Nectaris (region N, $\xi = 0.55$, $\eta = -0.25$) southeast of Theophilus is darker (lower albedo) than its surroundings and is therefore elevated in temperature by about 3°K. These effects can be seen in a thermal image (see Fig. 5).

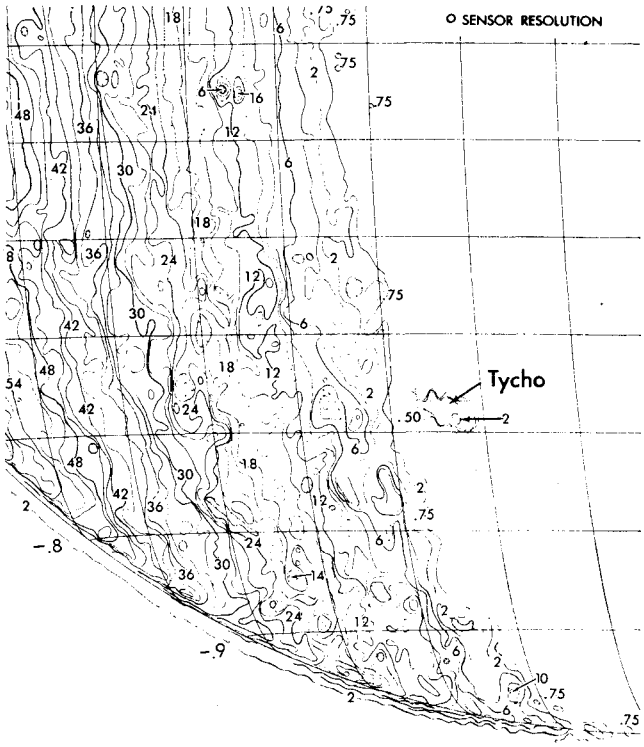

QUADRANT III PHASE ANGLE 112°

Contour Number	Temperature °K	Contour Number	Temperature °K	Contour Number	Temperature °K
.50	143.9	30	260.7	62	304.2
.75	150.7	32	264.1	64	306.4
2	169.7	34	267.3	66	308.6
4	186.4	36	270.5	68	310.7
6	197.7	38	273.5	70	312.8
8	206.7	40	276.4	72	314.9
10	214.2	42	279.2	74	317.0
12	220.7	44	282.0	76	319.0
14	226.6	46	284.7	78	321.0
16	231.9	48	287.3	80	322.9
18	236.8	50	289.9	82	324.9
20	241.4	52	292.4	84	326.8
22	245.7	54	294.8	86	328.7
24	249.7	56	297.2	88	330.5
26	253.6	58	299.6	90	332.4
28	257.2	60	301.9	92	334.2

Fig. 6 Isothermal map of the southwest quadrant of the illuminated portion of the moon at phase of 111° 40′.1 for $13^{H}\ 00^{M}$ UT on Oct. 11, 1963. Note that the crater Tycho is 170°K one day after sunset and its environs are less than 144°K.

In Saari and Shorthill's simultaneous isothermal and isophotic contour maps,[15] the position error in the various grid fits was about 2 arcsec. Figure 6 shows a portion of an isothermal contour map with calibration data. The isophotic contour maps (e.g., Fig. 7) are useful in the study of the effect of albedo variations on brightness temperatures.

Radiometric lunation curves for the center of the moon and for points at ±30° longitude along the equator are plotted in Fig. 8. The successful landing of Surveyor spacecraft provided the opportunity of making in situ temperature measurements. A temperature sensor was imbedded in the outboard face of a well-insulated electronic compartment. It was possible to infer the temperature of the local lunar surface during the lunar day, for several days after sunset and during an eclipse. During the daytime there was general agreement with the Earth-based data; both sets of data show a higher temperature before local noon, which is to be expected from directional effects of lunar thermal emission. The first results obtained from the Surveyor series are shown in Fig. 9. Detailed results of the Surveyor temperature measurements have been reported by the Surveyor thermal working group.[27–29]

The moon does not radiate infrared energy uniformly in all directions. Pettit and Nicholson found the temperatures along the equator at full moon vary as $\cos^{1/6}\theta$ (where θ is the angular distance to the subsolar point) and not as $\cos^{1/4}\theta$ as expected from a Lambertian surface. This was qualitatively explained by the roughness of the surface. Recent analysis of the directional effects on the full moon reveals that $\cos^{1/6}\theta$ is only an approximation to the experimental values, particularly near the limb. The variation of brightness temperature over the full moon has been studied by considering the data statistically. A least-squares fit to the statistical data is represented by the equation $T(°\mathrm{K}) = 324.2 + 72.6\cos\theta$. In Fig. 10, the statistical distribution of brightness temperature for the full moon is compared with the $\cos^{1/6}\theta$ variation. The variation of brightness temperature at full moon in the N-S direction from the disk center is shown in Fig. 11. Also shown in Fig. 11 is the variation in brightness temperature along the equator for the first and third quarter moon. The theoretical $\cos^{1/4}\theta$ variation is followed for quite a distance from the subsolar point, but as the terminator is approached the temperature rises above this theoretical value.

An extensive study was performed on isothermal contour maps through a lunation to obtain a better understanding of the directional characteristics of thermal emission. It was found to depend in a rather complicated way on the elevation angle of the sun and the observer's azimuth and elevation angles.[30] The data were studied in terms of a "thermal coordinate" system where the subsolar point is taken as the north pole (90° thermal latitude) and the terminator, the equator (0° thermal latitude). Thermal longitudes, great circles through the pole, are measured counter-clockwise around the subsolar point, zero longitude (the thermal meridian) passing through the disk center. The sketch in Fig. 12 shows the grid system for a scan made at a phase angle of 25° 37′ after full moon Brightness temperatures were measured every 10° in thermal latitude and longitude. Along a particular latitude where the sun angle is constant, the temperatures, in the absence of directional effects, should be constant, and in Fig. 12 the variations are indeed small for higher latitudes.

In a special study, the brightness temperatures along the thermal meridian for sun elevation angle every 10° were corrected for the sun-moon distance and for albedo variations. These data were then converted to elevation angle of the observer with respect to the surface and a least-squares polynomial fit was made for the values. In Fig. 13, for an observer on the surface, the 90° observer elevation angle corresponds to looking down vertically at the surface, 0° to looking at the horizon with the sun to his back, and 180° looking at the horizon into the sun. For sun elevation angles of 10° to 30°,

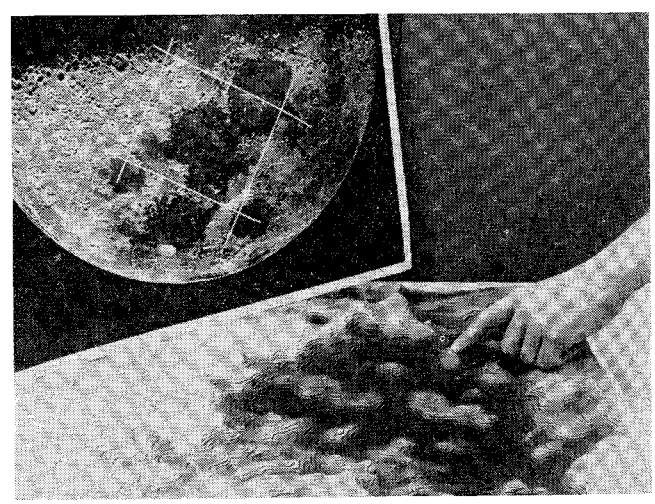

Fig. 7 Relief representation of the full-moon isophotic contours over the region of Mare Tranquilitatis. The crater indicated is Plinius.

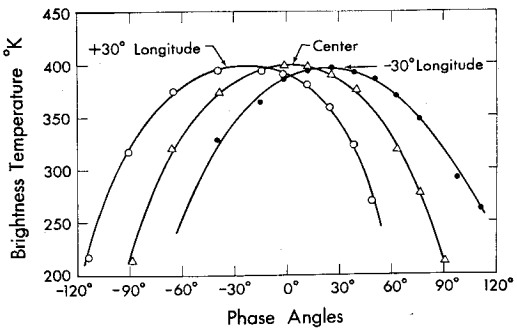

Fig. 8 Radiometric lunation curves for three points along the lunar equator.

the highest temperatures are obtained on the horizon, whereas for the higher elevation angles, the highest temperatures are obtained at observer elevation angles somewhat lower than the sun angle. Since the data were taken along the thermal meridian, the line of sight is in the plane defined by the surface normal and the sun.

The directional factor with the sun at 60° elevation can also be plotted in terms of an azimuth-elevation coordinate system; the azimuth is zero in the direction of the sun. The directional factor is defined as the ratio of the observed brightness temperature to the Lambert temperature of the surface. This factor was determined over the lunar disk at points where the sun was at 60° and the appropriate azimuth and elevation were calculated. A spherical harmonic fit to these data points is shown in Fig. 14. The highest brightness temperature (4.3% above the Lambert temperature) is obtained for 0° azimuth (looking toward the sun) at 47° elevation, somewhat below the sun. The lowest temperature is found at 180° azimuth and 0° elevation. In general, high values of brightness temperature are obtained when the angle defined by the sun and emission being measured (lunar phase angle) is small, and low values are obtained when the phase is large.

Another example of the directional factor is shown in Fig. 15, in terms of the sun elevation angle along the thermal meridian and the observer's elevation angles. The plot of the subsolar point variation with phase is, therefore, the upper boundary of the figure (sun at 90°), and the lower boundary is the terminator (sun at 0°). The directional data at various sun angles were used to interpret the Surveyor temperature measurements[28] when the lunar surface was illuminated by the sun.

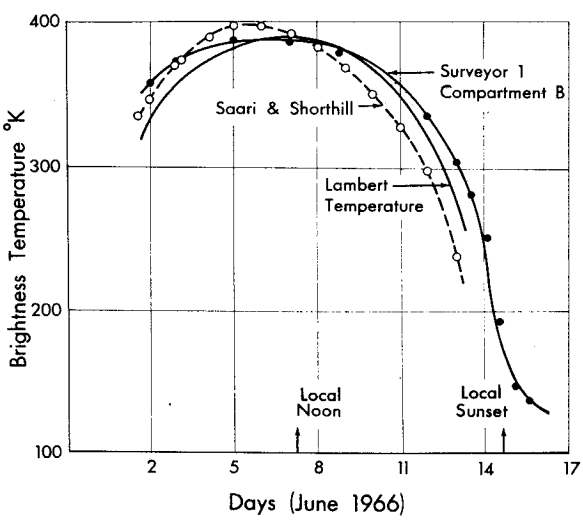

Fig. 9 Lunation temperature curves for the Surveyor I site. The Lambert temperature is the temperature a perfectly insulating Lambert surface with unit emissivity would come to if it absorbed the same amount of radiation as the surface under consideration.[27]

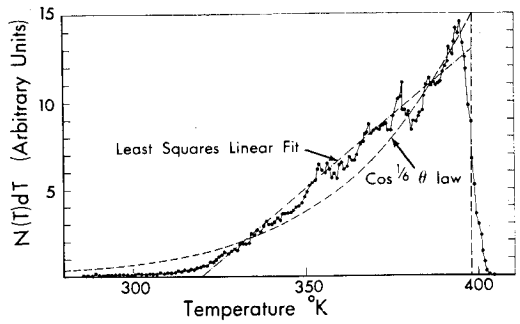

Fig. 10 Statistical distribution of brightness temperatures for the full moon disk. Fluctuations result from variations in the average albedo.

Nighttime Infrared Moon

The thermal response of the lunar nighttime surface is not well determined at this time. An example of data used to infer the midnight temperature is shown in Fig. 16 along with direct measurements of the antisolar point. The data are plotted in terms of days after local sunset. There are differences in the extrapolated equatorial scan data, which may be caused by drifts in the sky background. Also shown are the Sinton value of 122° ± 3°K, the Shorthill and Saari value of 99°K, and the Low[23] value of 90°K. The value of 106°K was determined by extrapolating the Murray, Wildey[20] data. The Pettit and Nicholson value was corrected by Saari[31] 108°K. Ingrao[32] has suggested that the curve of Murray and Wildey should be shifted by 5 hr toward the terminator. The extrapolation to the midnight value then becomes 104°K and was shown shifted that way in the previous Fig. 4 along with the nighttime results from Surveyor V which gives a value of 116°K.

An isothermal map of the unilluminated part of the third quarter was constructed by Wildey, Murray, and Westphal[22] where they reported over 100 nighttime anomalies, most of which correspond with hot spots found on the eclipsed moon. Two examples of scan line data across a nighttime anomaly are shown in Fig. 17. The general cooling of the environs of Copernicus can be seen as well as the anomalous cooling of the

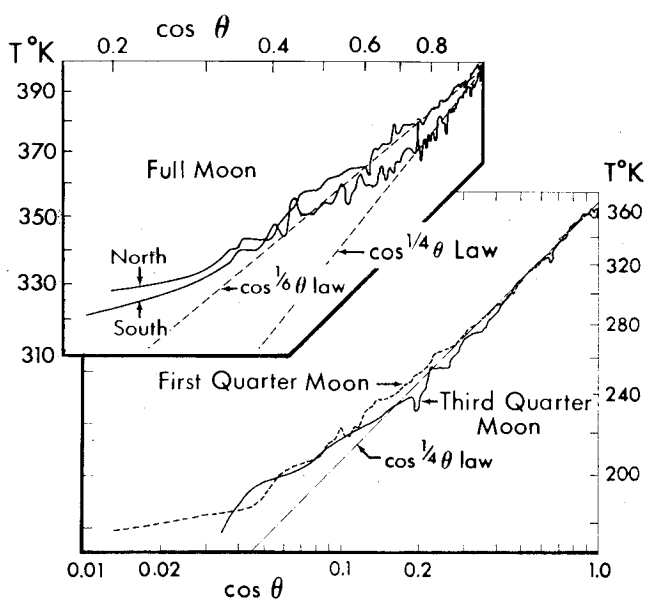

Fig. 11 Variation of brightness temperature in the N-S direction from the disk center are taken from the full-moon scan at phase angle of −2° 16′.1. The lower graph shows the temperature in the E-W direction along the equator at first- and third-quarter moon. Fluctuations are caused by variations in the average albedo and shadowing.

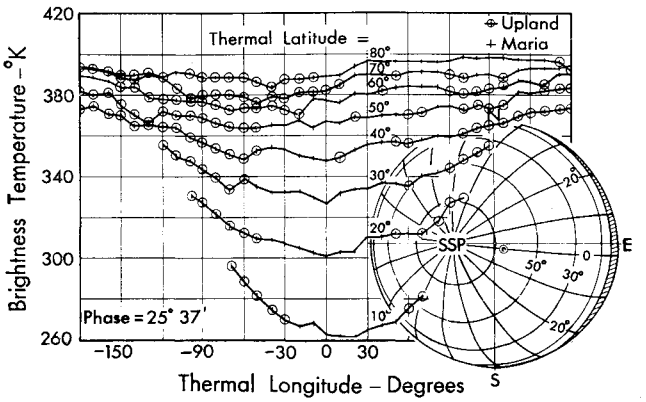

Fig. 12 Brightness temperature vs thermal longitude for lunar phase 25° 37′. Variations are caused by albedo differences and shadowing. The sketch shows the thermal coordinate system.

crater itself. The area of thermal enhancement extends beyond the crater as it does during an eclipse. It is surprising that there is no evidence of thermal structure in the crater or on the rims as there is during an eclipse. The crater Tycho, however, does show evidence of nighttime thermal structure in the infrared images of Hunt, Salisbury, and Vincent.[33]

With the rapid scan system of Saari and Shorthill,[15] isothermal maps of Tycho were obtained for three different times after sunset, one of which (~12 hr after sunset) was shown in Fig. 6. The lunation temperature curve (Fig. 18) for Tycho was determined from the isothermal contour maps.[15] The brightness temperature departs somewhat from the insolation because of directional effects explained previously. The three values following sunset are reliable. The two presunrise data points cannot be considered as reliable, since they were obtained by averaging all the data points within the crater. Post-midnight temperature measurements require extremely sensitive instrumentation. Frank Low,[23] however, using the 17.5- to 22-μ window and cancelling the sky background with a differential method, has measured temperature down to 70°K on the lunar surface. Figure 19 shows a typical scan of the derivative of the intensity profile across the nighttime surface. The bright limb and terminator show off-scale deflections. Thermal structure is indicated by the variations in the signal. Note that the sky noise has been almost completely eliminated. The point labeled "Hot Spot" reported by Low near the southeast limb has been tentatively identified from the eclipse data as Schomberger *F*.

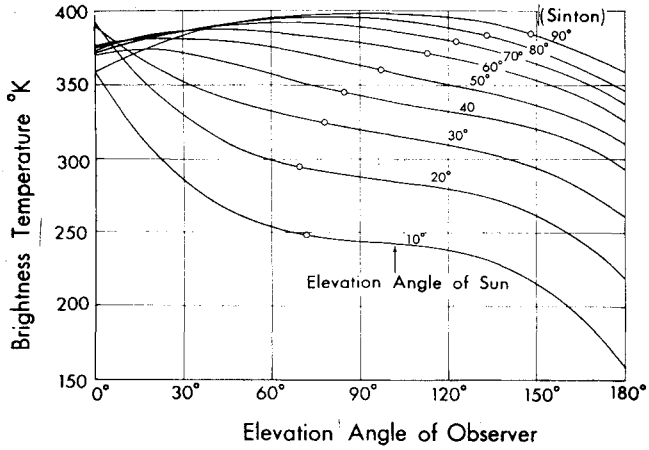

Fig. 13 Brightness temperatures vs observer's elevation angle to the surface with the sun at different elevation angles. The data for 90° sun angle are taken from Sinton's[4] observations of the subsolar point. The Lambert temperatures are indicated by open circles.

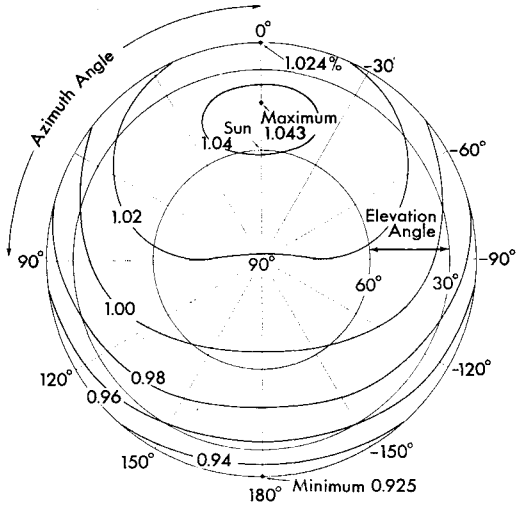

Fig. 14 Contours of directional factor (ratio of observed temperature to Lambert temperature) for the sun at 60° elevation.

Eclipse Infrared Moon

Perhaps the best summary of the observational results obtained for the eclipsed moon is represented by an image reconstructed from the scan line data of Saari and Shorthill.[34] Although images represent the data in only a qualitative manner, the major results are indicated. Figure 20 shows the thermal emission from the moon during totality at a resolution of 10 arcsec ($\frac{1}{200}$ the lunar diameter). The north line is inclined at 30° to left of center in the upper left portion of the figure. The bright spots number about 1000 and have been referred to as "hot spots" in the literature. The large spot $\frac{1}{5}$ the way from the bottom is Tycho; the other large spot to left of center is Copernicus. In addition to these two ray craters already known to be thermally anomalous, all the major ray craters such as Aristoteles, Dionysius, Langrenus, Menelaus, and Stevinus are also anomalous. Besides these localized hot spots; extended regions of thermal enhancement can be seen on the image which are related to certain maria and portions of maria. One example is Mare Humorum opposite Tycho to the left.

Figure 21 shows the normalized eclipse cooling curve for the center of the lunar disk (eclipse time is normalized to the penumbral duration). The curve is not significantly different from that obtained by Pettit in 1939. An eclipse cooling curve for any point on the earthside hemisphere may be obtained from the data of Ref. 35. Isothermal contours have been constructed for the seven eclipse scans and for the full moon before the eclipse. The isothermal contours obtained at full moon just prior to onset of the eclipse for the crater Tycho are illustrated in Fig. 22. A lunar Orbiter photograph (not at full moon) of Tycho in Fig. 23 has the seleneographic latitude and longitude superimposed. The full-moon tem-

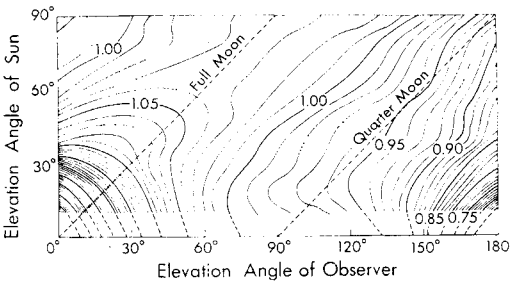

Fig. 15 Contours of directional factor for points on the thermal meridian (the great circle through the disk center and the subsolar point).

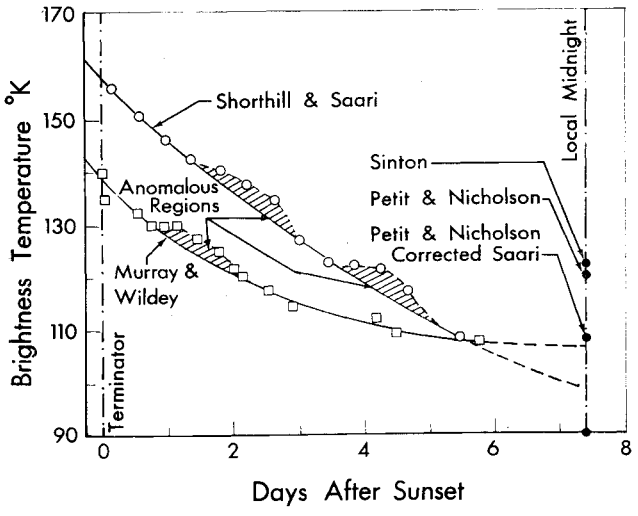

Fig. 16 Equatorial brightness temperature vs days after local sunset. The anomalous regions are due to maria or hot spots.

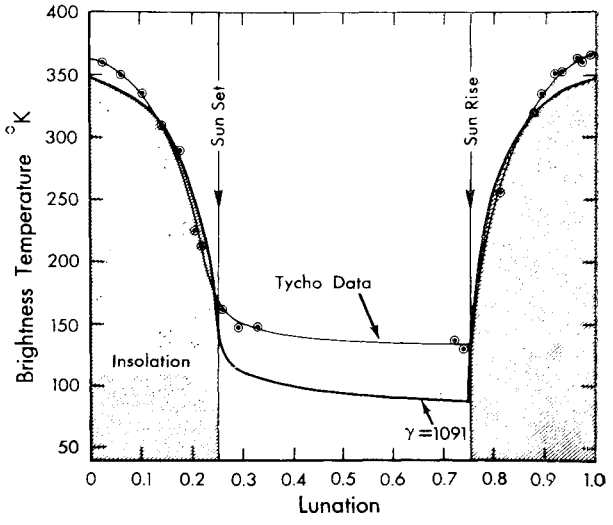

Fig. 18 Lunation temperature curve for the crater Tycho The curve departs from the insolation because of directional effects.

perature of Tycho is slightly below its environs because of its relatively high albedo. As Tycho cools during the eclipse, a region around the southeast interior which was the coolest part of the crater at full moon (359.6°K which is 9.1°K below its environs) becomes the warmest part during totality (227.1°K which is now 51°K above its environs), and the anomalous region extends beyond the crater by about half a crater diameter (Fig. 24). Three relative maxima appear in the thermal structure, one near the central peak, one along the west interior, and one on the southeast floor or interior wall. Copernicus has similar characteristics. Detection of thermal structure in smaller craters was limited by the resolution used in the measurements.

The eclipse cooling curves for Tycho and its environs are shown in Fig. 25. The data point at normalized time 3.5 is tentative because of certain calibration problems. Each point in Fig. 25 represents the average of ~50 data points reading across the crater. During the penumbral phase of the eclipse the cooling curves depart from the insolation curve because of the thermal inertia of the surface.

A special study was done on 83 of the hot spots with the largest signal differences over their environs.[35] Many of these

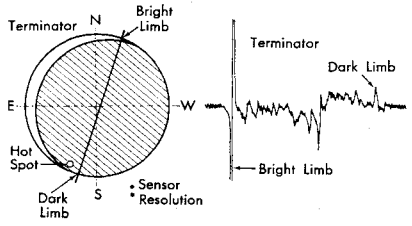

Fig. 19 An example of a scan across the nighttime surface showing the derivative of the intensity profile at 20μ.[23] The hot spot reported by Low has been tentatively identified as Schomberger F.

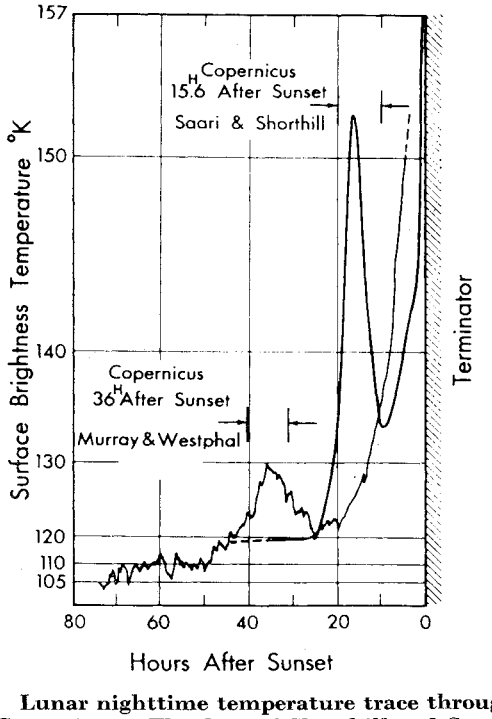

Fig. 17 Lunar nighttime temperature trace through the crater Copernicus. The data of Shorthill and Saari were replotted and appear abnormally smooth.

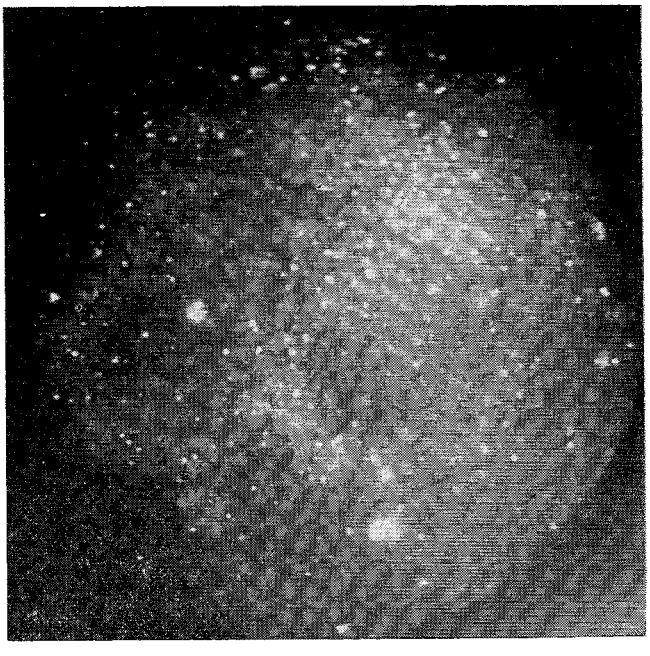

Fig. 20 Thermal image of the eclipsed moon during totality. The midpoint of the scan is 2^{H} 18.8^{M} UT, Dec. 19, 1964. Individual scan lines can be seen. The bright region in the lower right corner is caused by radiation from the side of the telescope.

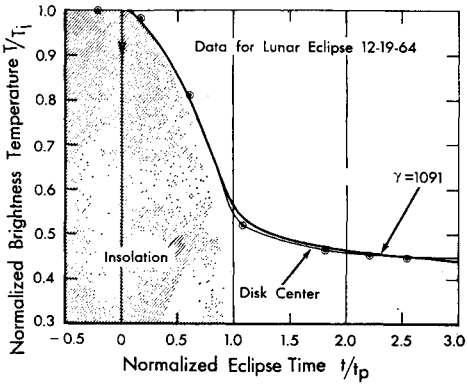

Fig. 21 Eclipse cooling curve normalized to initial temperature and penumbral duration. The constant properties model [$\gamma = (K\rho c)^{-1/2} = 1091$] plotted here assumes constant K (thermal conductivity), constant c (specific heat) with temperature and constant ρ (density) with depth.

were associated with craters smaller than the projected sensor diameter. An areal correction was made with the assumption that the hot spot was confined to the crater and the emission was uniform across the crater. The correction took into account the crater diameter, its projection onto the sensor diameter, and the relative signal difference above the environs on successive scan lines. The 30 most prominent areally corrected craters were ranked and are shown in Table 1.

Six are ray craters, 20 are craters with bright interiors, and 4 have bright rims. There are 5 in the uplands and 23 in the

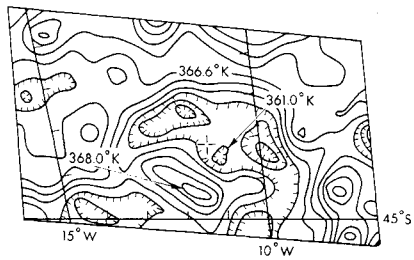

Fig. 22 Full-moon isothermal contours just prior to an eclipse. The northwest interior walls are warmer because the sun is more normal to the surface; similarly the northeast interior walls are cooler because the sun is more grazing.

maria. A plot of areally corrected signal difference vs crater diameter is shown in Fig. 26 (68% of these hot spots are smaller than the sensor diameter). The plot represents the boundary of a general distribution for a large number of hot spots. It is expected that as the resolution is improved a larger number of

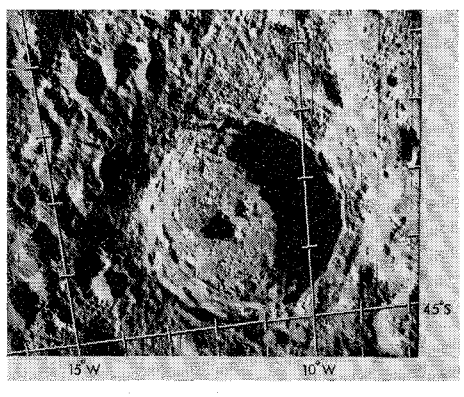

Fig. 23 Lunar Orbiter photograph of the crater Tycho. The thermal contours shown in Figs. 6, 22, and 24 can be compared to the features on this photograph.

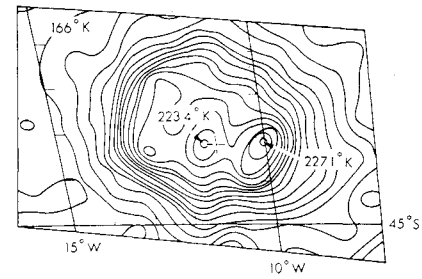

Fig. 24 Isothermal contours over Tycho during the totality of the lunar eclipse of Dec. 19, 1964 at 3^H 2.8^M UT. The anomalous region extends beyond the crater by at least half a crater diameter.

hot spots will be observed. There is an upper limit on the signal difference over the environs if the thermal parameter γ is not less than 20 (bare rock). Mösting C was observed to have a ΔT of 28°K above its environs, whereas the areally corrected temperature difference $\Delta T_c = 157$°K suggests the properties of bare rock. The Lunar Orbiter spacecraft photographed certain of the hot spots with high resolution. The pictures indicate that these craters are among the younger features on the lunar surface. In general, they appear to be rougher and to have a higher number of boulders inside and around the rims than older craters; e.g., Fig. 27 shows that Mösting C has sharp features with an interior looking like bare rock, and the ejecta blanket is covered with boulders.

A classification of the 330 hot spots revealed that most of them are associated with regions or craters with high albedo. Table 2 lists the preliminary finding; of those listed, two-thirds fall in the lunar maria and one-third in the uplands. The density distribution of all the hot spots over the hemisphere is shown in Fig. 28.[36] The greatest concentration is found in Mare Tranquillitatis and in a region between Kepler and Aristarchus. Several different randomness tests showed that the probability that the high Mare Tranquillitatis concentration (marked H) would occur by chance was one in 50000.

The thermal contours obtained during the last scan in totality were drawn onto the 20 AIC charts* for the "Apollo Band," i.e., the region ±8° in latitude and ±50° in longitude.[26] The original contours were drawn by computer along with the appropriate librated grid in longitude and latitude. The formal rms error in the librated grid was 2.3 arcsec, or $\sim\frac{1}{4}$ of the sensor resolution. In the grid-fitting process already described, 45 known hot-spot features distributed over the disk were used. The contours were manually transferred

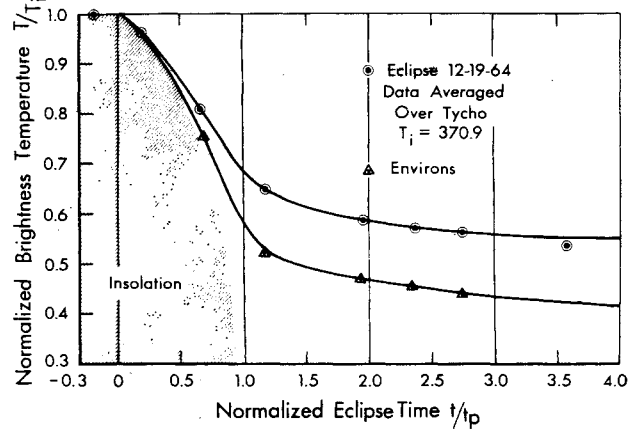

Fig. 25 Normalized eclipse cooling curve for Tycho.

* Each of these charts, constructed by U.S. Air Force Aeronautical Chart and Information Center, St. Louis, covers 10° in longitude and 8° in latitude at a scale of 1:500,000.

Table 1 Ranking of 30 prominent anomalies on the eclipsed moon

No.	Crater	Diam, km	No.	Crater	Diam, km
1	Mösting C	3.8	16	Egede A	12.5
2	Piton B	4.8	17	Laplace A	9.7
3	Messier A	13.6	18	Nicollet	15.2
4	Bunch B	6.7	19	Mösting A	13.0
5	Jansen E	7.0	20	Mason C	12.3
6	Torricelli	6.9	21	Cauchy	12.3
7	Draper C	7.7	22	Gambart C	12.2
8	Maraldi B	7.4	23	Carlini D	9.3
9	Moltke	6.4	24	Eudoxus A	14.1
10	Plato M	8.3	25	Pico B	11.4
11	Guericke C	10.9	26	Cephus A	12.5
12	Flamsteed B	9.4	27	Hesiodus B	10.2
13	Taruntius H	8.3	28	Janssen K	15.5
14	Jansen F	9.4	29	Bode A	12.3
15	Marius A	16.0	30	Carlini	11.4

onto each AIC chart. An example of one such chart is Wichmann AIC 75B 40° to30° W longitude; 0°–8° S latitude (see Fig. 29). There are relatively few hot spots in this region of Oceanus Procellarum. The most prominent is Lansberg D (30.°6 W, 3.°0 S) with a ΔT of 27.5°K. Because of their unusual appearance, they may indicate a process different from those forming other features. Figure 30 shows such a feature in the ray system of Kepler at 42.°90 W, 7.°08 N. This

Table 2 Classification of 330 thermal anomalies on the eclipsed moon

Classification	%
Ray craters	19.4
Craters with bright interior at full moon	41.8
Craters with bright rims at full moon	23.3
Craters not bright at full moon	0.6
Bright areas with much smaller crater	3.6
Bright areas (like ridges)	3.9
Bright areas (no feature)	1.2
Position unidentified or questionable	6.3

feature was detected on two successive scan lines. The two peak temperatures as well as the environs were plotted (Fig. 31). It is apparent that the peak temperature depends on just how the sensor passes through the hot spot. An areal

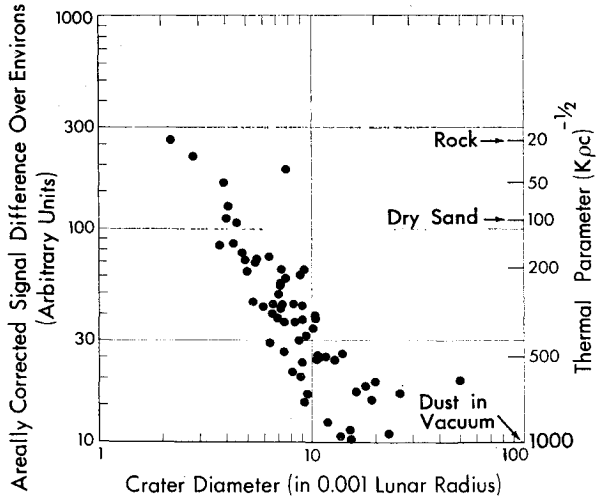

Fig. 26 Hot-spot signal difference vs crater diameter. The resolution of the sensor corresponds to 0.01 of the lunar radius. The signal difference, when compared to the theoretical cooling of a constant properties model of the lunar surface, corresponds to values of the thermal parameter, $\gamma = (K\rho c)^{-1/2}$.

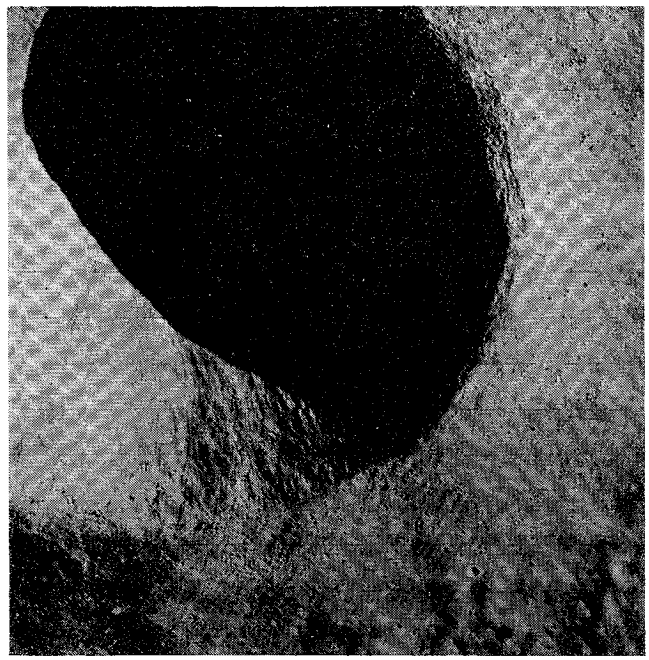

Fig. 27 Lunar Orbiter photograph of Mösting C (8°.1 W, 1°.8 N). The crater diameter is 3.84 km.

correction was made on the assumption that the source was 18 km in diameter. Since the magnitude of the two signals on successive scan lines depends on the geometry of intersection of the sensor and hot spot, the temperature of the "feature" can be determined. The areal correction produced a smooth cooling curve that is parallel to the environs curve.

Table 3 Characteristics of 98 hot spots in the Apollo Band identifiable with craters in Ref. 37

Crater[a] class	Mare	Boundary	Upland	Class total
1	58	8	19	85
2	7	1	3	11
3	1	0	0	1
4	0	0	1	1
5	0	0	0	0
Total craters	66	9	23	98

[a] Class 1—complete and sharply defined rims, Class 2—rims blurred, Class 3—rim broken, Class 4—ruins, Class 5—battered and fragmentary.

Radar images in the equatorial band have been constructed by the MIT Lincoln Laboratory.[38] These measurements made at 3.8 cm show some remarkable correlation with the infrared data (Table 4). Their resolution was substantially better than any of the infrared data. No radar features were listed closer than 23° from the center of the lunar disk for reasons described in Ref. 38. When this difficulty is removed, additional correlation should be expected within 23° of the disk

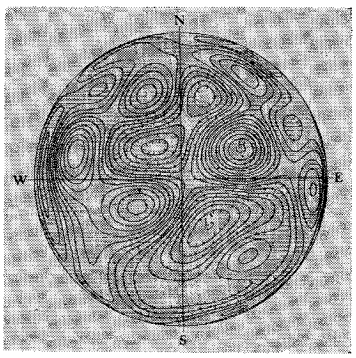

Fig. 28 A spherical harmonic fit to the density of 1011 hot spots on the lunar hemisphere with a contour interval of 0.7 hot spots per 10^5km^2 The mean in the distribution 5.34. A high of 14 (indicated by H) is located in Mare Tranquillitatis. The minimum representing zero hot spots per 10^5 km^2 is labeled with an L.

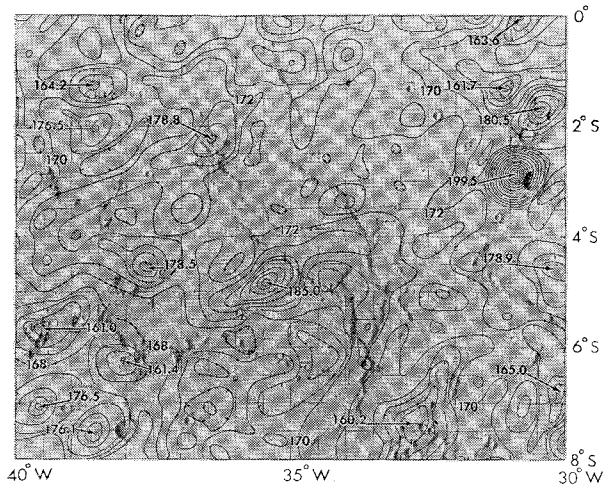

Fig. 29 Isothermal contours on the AIC base. At 35°.5 W longitude and 5°.3 S latitude is a hot spot for which no related visible feature can be identified.

center. In several instances the apparent source of the hot spot is a small region of high albedo sometimes with small craters similar to those in Fig. 30. In most cases, however, the major radar enhancements listed in Table 4 can be related to moderate-sized craters.

The correlation between the radar enhancements on hot spots is interesting, because radar is sensitive only to structure of the surface and not to thermal emission. For example, a region that is covered with rocks and/or characterized by exceptionally dense surface material will exhibit enhanced radar backscattering and anomalous eclipse cooling. This would suggest that a method for detecting an internal heat source would be to observe areas that are not radar enhancements but have anomalous cooling during an eclipse or the lunar nighttime. Considering, however, the moon's highly insulating layer, Saari[39] has shown that it is very unlikely that subsurface heat source can be detected with infrared radiometric measurements. Actually, the search for internal heat sources could perhaps best be done by high-resolution microwave radiometry from an orbiting lunar spacecraft. The observations of lunar transient events described by Middlehurst[40] may be evidence of internal activity. Many of these events took place in regions which are not associated with thermal anomalies such as Alphonsus, Gassendi, Plato, and Sabine. A few of them, however, did occur in regions that are thermal anomalies, such as Tycho, Aristarchus, and Messier A. There does not seem to be any strong correlation between transient lunar events and the eclipse hot spots. It is possible that most of the hots spots are produced by concentrations of rocks on the surface, in which case the eclipse contours are in reality

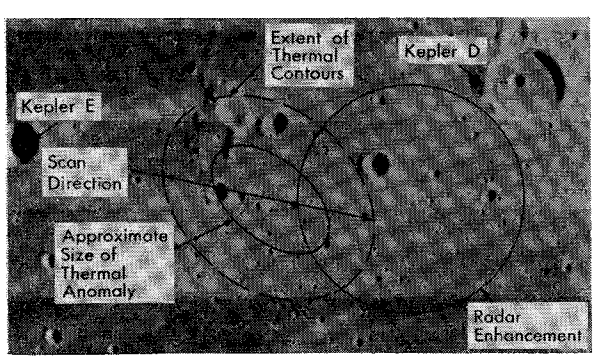

Fig. 30 A "no-feature" hot spot photographed by Lunar Orbiter IV (Frame 144). The temperature was 18.2°K above that of the environs, and the 3.8-cm radar enhancement was 30 km in diameter. Several small craters (<3 km) are seen in the enhanced region.

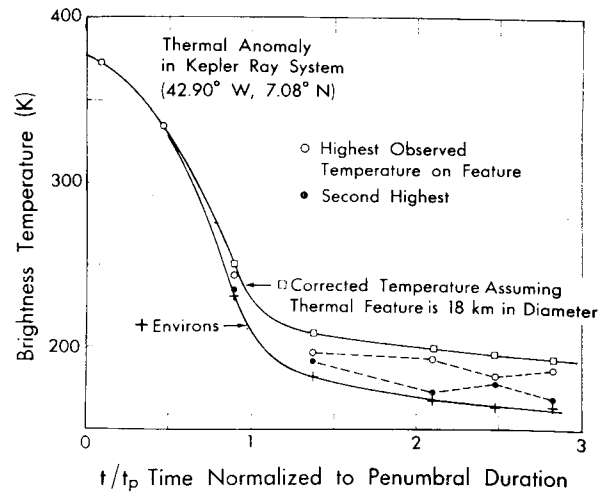

Fig. 31 Eclipse cooling curve for the "no feature" hot spot shown in Fig. 30.

"rock detectors." Lunar Orbiter, Surveyor, and Apollo photographs show that rocks are commonly found in and around craters, on certain ridges, and in some of the rilles.

It is somewhat difficult to compare different areas over the moon on an equal basis using the eclipse isothermal contour charts for two reasons. First, the isotherms show a drop off toward the limb because of a lower initial temperature T_i, and second, the temperatures in the west are lower than in the east, because westerly points have cooled longer. Figure 32 shows some preliminary results of removing these two effects to produce a "flattened moon." The trace passes through Mare Humorum between data points 340 and 400, through Heinsius A to data point 560 and through Tycho between data points 590 and 640. Similar data were obtained for the entire set of scan lines, and a contour map of $\Delta T/T_i$ was constructed for further study.

Theoretical Model

Previous theoretical models describing the temperature variation of the typical lunar surface were unable to fit simultaneously the lunar nighttime and the eclipse cooling data. Recently a "particulate model" has been developed by Winter and Saari[12] which fits both sets of data (Figs. 33 and 34).

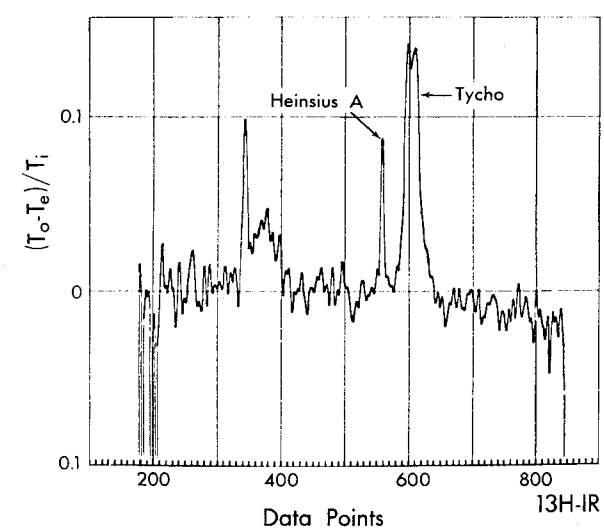

Fig. 32 The trace for the "flattened moon" (T_0 is the observed temperature, T_e is the empirically determined average lunar surface temperature, and T_i is the initial full-moon temperature).

Table 4 Location of relatively large regions of strongly enhanced local roughness from the 3.8-cm radar data[38] and related infrared hot spots[a]

Radar				Infrared				
	Location		Approx.		Location		Crater	
Site	Long., deg	Lat., deg	diam, km	Crater name	Long., deg	Lat., deg	diam, km	ΔT, K
A	−68.7	−12.9	25	Bright spot near Rocca Ab	−68.3	−12.3	...	11
B	−67.0	−14.7	20	Bright spot below Rocca Fa	−66.8	−14.3	...	8
C	−64.7	−8.0	25	Grimaldi G (?)	−64.8	−7.7	5.98(?)	14
D	−59.8	−13.5	30	Sirsalis F and/or J	−60.0	−13.1	6.82	16
E	−52.3	−3.5	30	Flamsteed Gc	−52.5	−3.2	4.96	22
F	−50.5	−1.2	20	Unnamed crater	−50.3	+0.1	3.0(?)	9
G	−48.0	+3.9	35 × 18	Suess	−47.7	+4.4	9.14	32.4
H	−44.9	−15.0	30 × 20	Gassendi F	−45.2	−14.9	4.85	17
I	−42.3	+7.0	30	Small craters (Fig. 42)	−42.9	+7.1	...	18.2
J	−40.3	+1.0	30 × 15	Encke X	−40.2	+0.9	3.53	17.1
K	−36.8	−12.8	18	West of Herogonius Ec	−36.7	−12.7	...	7
L	−25.8	+1.8	15	Reinhold NA	−24.5	+1.9	2.24	20.0
M	+32.8	0	100 × 30	Near Censorinus	+32.7	+0.4	3.82(?)	25.5
N	+36.2	−6.8	15	Capella C, CA, RA (?)	+36.0	+6.0	...	8.8
O	+41.4	+3.1	15	Secchi B	+41.6	+3.8	5.25	14.8
P	+47.2	−2.0	50	Messier A	+46.9	−2.0	13.00	46.0
Q	+51.7	+0.6	35	Taruntius K	+51.5	+0.7	3.01	26
R	+53.3	+12.3	18	East rim of Lick	+53.1	+12.4	...	8

[a] ΔT is temperature above environs.

They describe their model as a cubic array of cubes; each is in contact with its immediate neighbor only along common edges, so that the void fraction is 0.5, and the particles (cubes) are assumed to be opaque throughout the relevant spectral region. They considered each individual particle approximately isothermal. The effect of contact conduction is included using the results from Watson's experiments[41] with evacuated powders. In the model, specific heat is a function of temperature. Winter and Saari have plotted the predicted nighttime temperature for the particulate model and constant-properties model,† (see Fig. 33). The curves are compared with observed lunar nighttime temperatures. For the constant-properties model the best value for nighttime cooling is a γ of 800 (Fig. 33) whereas for an eclipse, a γ a 1300 gives the best fit (Fig. 34). The new measure of eclipse cooling devised by Winter and Saari and plotted in Fig. 34 is the "differential energy parameter." This parameter P, which permits more meaningful comparison, particularly during the penumbral phase of an eclipse, is defined by the equation

$$P = (T/T_i) - I(\tau)$$

where $\tau = t/t_p$ is time normalized to the penumbral duration starting with the beginning of the penumbra, T_i is the full moon temperature at $\tau = 0$, and $I(\tau)$ is the solar flux normalized to the full moon value at $\tau = 0$. In Fig. 34, the black dots represent the measurements of Shorthill and Saari.

The foregoing brief description of the particulate model refers to the typical lunar surface. We know, however, that rocks are present on the lunar surface. It is expected that their thermal behavior during a lunation and an eclipse will be different than that of the typical lunar surface. Roelof[42] investigated the thermal behavior of rocks and found that during most of a lunation the small ($\lesssim$10 cm) rocks are slightly cooler than the general surface and are approximately isothermal. During sunrise and sunset these small rocks will have considerably higher temperatures than the typical lunar surface, which may account for some of the directional effects (i.e., limb brightening at full moon). The thermal response through a lunation of a 1-m basaltic cube on the lunar equator is shown in Fig. 35; here, isothermal conditions do not hold, and each face has a different lunation curve. Studies of small

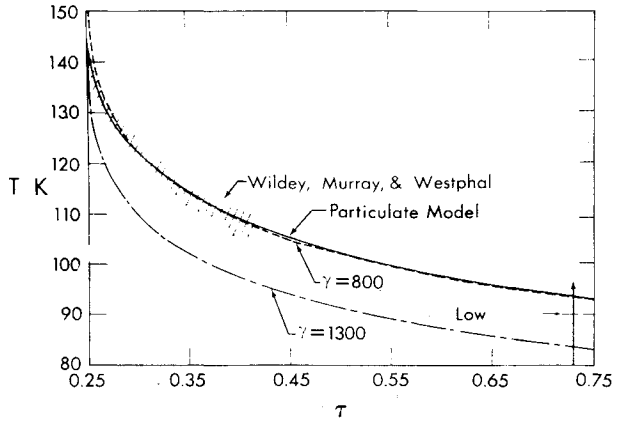

Fig. 33 Theoretical predictions of nighttime temperatures from the cube model after Winter and Saari[12] and the constant-properties model. Time, τ, is normalized to a lunation and is measured from local noon.

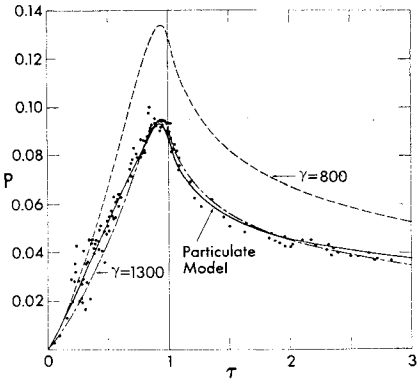

Fig. 34 Theoretical predictions of differential energy parameter from the particulate model[12] and the constant-properties model. Time τ is normalized to the penumbral duration and is zero at the state of the penumbra. The data points (dots) are from the eclipse data of Ref. 35.

† The constant-properties model is characterized by a single parameter, γ (gamma) = $(K\rho c)^{-1/2}$ (thermal parameter) in cal^{-1}cm^{2}sec$^{1/2}$°K, where K = thermal conductivity in cal cm^{-1} sec^{-1} °K^{-1}, ρ = density in g cm^{-3}, and c = specific heat in cal g^{-1} °K^{-1}.

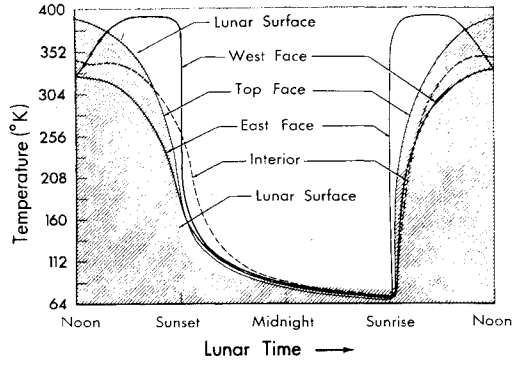

Fig. 35 Lunar temperature curves for the faces of a 1-m basaltic cube on the lunar equator after Roelof.[41]

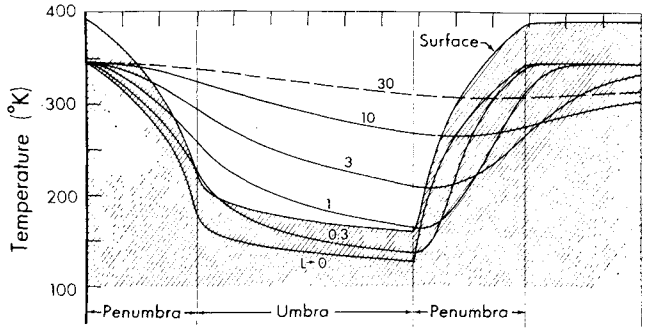

Fig. 36 Eclipse temperature curve for small rocks (L = 0 to 30 cm) at the apparent center of the lunar disk after Roelof.[41] The shaded area represents the typical lunar surface.

rocks during an eclipse were also performed (Fig. 36); the 30-cm curve is dashed, because the isothermal assumption probably is poor at this size.

Roelof concluded that at sunset and sunrise the gross lunar topography is probably a more important factor in temperature anomalies, whereas the fraction of the surface covered by small rocks is too small to exhibit the effect of rock temperatures at noon. Likewise, the enhancement in brightness temperature during an eclipse is estimated to be not large (~15°K) on the basis of the rock-size distribution deduced from the observations of Surveyor I and III. Thus, small rocks are ruled out as the cause of the larger hot spots (ΔT = 50°K) during an eclipse. This, however, may not be the case if the rock distributions near hot spots differ markedly from the Surveyor sites. Further, Roelof states that local thermal measurements by a spacecraft could be influenced by small rocks. The distribution as well as location of rocks larger than 10 cm must be known, since the energy radiated is a sensitive function of the distribution.

Concluding Remarks

Many characteristics of the "infrared moon" are known and have been described in this paper. The brightness temperature of the surface during the lunation is easily determined from the surface albedo and a knowledge of the insolation. The directional properties of thermal emission, however, were not predicted and required experimental measurements for their determination. These directional properties were important for the interpretation of the Surveyor results. Recent theoretical work by Winter,[43] has shown that a certain distribution of craters with a depth-to-diameter ratio of 1:2 will reproduce the general form of directional emission from the lunar surface.

The eclipse cooling of the average lunar surface has been modeled by various investigators. The particulate model developed by Winter and Saari[12] has been the most successful. In order to explain the hot spots, a distribution of rocks similar to those found on Surveyor VII were used by Winter[45] successfully to explain the slower cooling rates characteristic of the eclipse hot spots.

Several questions remain concerning the thermal data. For example, many of the hot spots cannot be identified with topographical features. In some cases these hot spots are also radar enhancements. Another question to be answered is the cause of the thermal enhancements during an eclipse in the maria or parts of mare. Outstanding in this respect is Mare Humorum which was found to be about 10° warmer than its environs. Mare Humorum, therefore, should be considered as a site for further high-resolution photography, a target for orbital remote sensing from lunar orbit, and a landing site for further exploration.

Many of these eclipse hot spots are observed by Earth-based telescopes to cool more slowly during the lunar nighttime. Some important questions are: What are the sunrise temperatures in these regions? Are there any regions that cool more slowly during the nighttime which were not observed during the eclipse? What is the temperature distribution within the hot spot? How large are those anomalies? In this regard, Allen and Ney[44] have recently reported the first of their findings on the possible nighttime temperature distribution in hot spots. They found Tycho, for instances to have a color temperature of 200°K, which indicates that the thermal anomaly is probably a combination of hot regions and cold regions, with the hot regions representing 2% to 10% of the total area.

As exploration of the moon continues, many of the foregoing questions may be answered, but it will not be surprising if new data also pose new questions.

References

[1] Rosse, L., "On the Radiation of Heat from the Moon," *Proceedings of the Royal Society of London*, Vol. 27, 1869, pp. 436–441.

[2] Pettit, E. and Nicholson, S. P., "Lunar Radiation and Temperatures," *Astrophysical Journal*, Vol. 71, No. 2, Feb. 1930, pp. 102–135.

[3] Zel'tser, M. S., "The Temperature of the Lunar Surface," *The Moon—A Russian View*, edited by A. V. Markov, University of Chicago Press, 1960, pp. 175–203.

[4] Sinton, W. M., "Temperature on the Lunar Surface," *Physics and Astronomy of the Moon*, edited by Z. Kopal, Academic Press, New York, 1962, Chap. 11, pp. 407–428.

[5] Shorthill, R. W., "Measurements of Lunar Temperature Variations During an Eclipse and Throughout a Lunation," *Proceedings of the Conference on Lunar Exploration, Bulletin*, paper VI, Virginia Polytechnic Institute, Engineering Experiment Station Series 152, Pt. A, Vol. 56, No. 7, May 1963.

[6] Wesselink, A. J., "Heat Conductivity and Nature of the Lunar Surface Material," *Bulletin of the Astronomical Institute, Netherlands*, Vol. 10, No. 390, April 1948, pp. 351–363.

[7] Jaeger, J. C. and Harper, A. F. A., "Nature of the Surface of the Moon," *Nature*, Vol. 166, Dec. 1950, p. 1026.

[8] Jaeger, J. C., "The Surface Temperature of the Moon," *Australian Journal of Physics*, Vol. 6, March 1953, pp. 10–21.

[9] Sinton, W. M., "The Moon," *Planets and Satellites*, edited by G. P. Kuiper, University of Chicago Press, 1961, pp. 438–441.

[10] Geoffrion, A. R., Korner, M., and Sinton, W. M., "Isothermal Contours of the Moon," *Lowell Observatory Bulletin No. 106*, Vol. V, No. 1, May 1960, pp. 1–15.

[11] Shorthill, R. W., Borough, H. C., and Conley, J. M., "Enhanced Lunar Thermal Radiation during a Lunar Eclipse," *Publication of the Astronautical Society of the Pacific*, Vol. 72, No. 429, Dec. 1960, pp. 481–485.

[12] Winter, D. F. and Saari, J. M., "A Particulate Thermophysical Model of the Lunar Soil," *Astrophysical Journal*, Vol. 156, June 1969, pp. 1135–1157.

[13] Sinton, W. M., "A Pyrometer for Planetary Temperature Measurements," *Lowell Observatory Bulletin No. 104*, Vol. IV, No. 16, Dec. 1959, pp. 260–263.

[14] Shorthill, R. W. and Saari, J. M., "Radiometric and Photo-

metric Mapping of the Moon through a Lunation," *Annales of the New York Academy of Sciences*, Vol. 123, Article 2, June 1965, pp. 722–739.

[15] Saari, J. M. and Shorthill, R. W., "Isothermal and Isophotic Atlas of the Moon," CR-855, Sept. 1967, NASA.

[16] Low, F. J., "Low Temperature Germanium Bolometer," *Journal of the Optical Society of America*, Vol. 51, No. 11, Nov. 1961, pp. 1300–1304.

[17] Hunt, G. R., Salisbury, J. W., and Vincent, K., "Lunar Eclipse: Infrared Images and an Anomaly of Possible Internal Origin," *Science*, Vol. 162, Oct. 1968, pp. 252–254.

[18] Pettit, E., "Radiation Measurements on the Eclipsed Moon," *Astrophysical Journal*, Vol. 91, May 1940, pp. 408–420.

[19] Saari, J. M. and Shorthill, R. W., "Isotherms of Crater Regions on the Illuminated and Eclipsed Moon," *Icarus*, Vol. 2, Aug. 1963, pp. 115–136.

[20] Murray, B. C. and Wildey, R. L., "Surface Temperature Variations During the Lunar Nighttime," *Astrophysical Journal*, Vol. 139, No. 2, Feb. 1964, pp. 734–750.

[21] Vitkus, G., Lucas, J. W., and Saari, J. M., "Lunar Surface Thermal Characteristics during Eclipse from Surveyors III, V, and after Sunset from Surveyor V," AIAA Paper 68-747, Los Angeles, Calif., 1968.

[22] Wildey, R. L., Murray, B. C., and Westphal, J. A., "Reconnaissance of Infrared Emission from the Lunar Nighttime Surface," *Journal of Geophysical Research*, Vol. 72, July 1967, pp. 3743–3749.

[23] Low, F. J., "Lunar Nighttime Temperatures Measured at 20 Microns," *Astrophysical Journal*, Vol. 142, No. 2, June 1965, pp. 806–808.

[24] Ingrao, H. C., Young, A. T., and Linsky, J. L., "A Critical Analysis of Lunar Temperature Measurements in the Infrared, *Harvard College Observatory of Science, Report 6*, April 1965.

[25] LaRocca, A. and Zissis, G. J., "Field Sources of Blackbody Radiation," *The Review of Scientific Instruments*, Vol. 30, No. 3, March 1959, pp. 200–201.

[26] Shorthill, R. W. and Saari, J. M., "Infrared Observations on the Eclipsed Moon," *Physics and Astronomy of the Moon*, 2nd ed., edited by Z. Kopal, Academic Press, New York, Chap. 9, to be published.

[27] Lucas, J. W., Conel, J. E., Hagemeyer, W. A., and Saari, J. M., "Lunar Surface Thermal Characteristics from Survey I," *Journal of Geophysical Research*, Vol. 72, No. 2, Jan. 1967, pp. 779–789.

[28] Lucas, J. W. et al., "Lunar Surface Temperatures and Thermal Characteristics: Surveyor 5 Science Results," *Journal of Geophysical Research*, Vol. 73, No. 22, Nov. 1968, pp. 7209–7219.

[29] Vitkus, G. et al., "Lunar Surface Temperatures and Thermal Characteristics," TR 32-2362, *Surveyor VI Mission Report—Part II: Mission Results*, Jet Propulsion Lab., Jan. 1968, pp. 109–123.

[30] Montgomery, C. G. et al., "Directional Characteristics of Lunar Thermal Emission," Document D1-82-0568, Nov. 1966, Scientific Research Labs., The Boeing Co.

[31] Saari, J. M., "The Surface Temperature of the Antisolar Point of the Moon," *Icarus*, Vol. 3, No. 2, July 1964, pp. 161–163.

[32] Ingrao, H. C., Young, A. T., and Linsky, J. L., "A Critical Analysis of Lunar Temperature Measurements in the Infrared," *The Nature of the Lunar Surface*, edited by H. Hiss, D. Menzel, and J. O'Keefe, Johns Hopkins, Baltimore, 1966, pp. 185–211.

[33] Hunt, G. R., Salisbury, J. W., and Vincent, R. K., "Infrared Images of the Eclipsed Moon," *Sky and Telescope*, Vol. 36, No. 4, Oct. 1968, pp. 2–4.

[34] Saari, J. M. and Shorthill, R. W., "Infrared and Visible Images of the Eclipsed Moon of December 19, 1964," *Icarus*, Vol. 5, No. 6, Nov. 1966, pp. 635–659.

[35] Shorthill, R. W. and Saari, J. M., "Nonuniform Cooling of the Eclipsed Moon: A Listing of Thirty Prominent Anomalies," *Science*, Vol. 150, No. 3693, Oct. 1965, pp. 210–212.

[36] Green, R. R., "An Analysis of the Distribution of the Major Surface Characteristics and the Thermal Anomalies Observed on the Eclipsed Moon," Document D1-82-0775, Jan. 1969, Scientific Research Labs., The Boeing Co.

[37] Arthur, D. W. G. et al., "No. 30 The System of Lunar Craters, Quadrant I," *Communications of Lunar and Planetary Laboratory*, Vol. 2, Sept. 1963, pp. 71–78; "No. 40 The System of Lunar Craters, Quadrant II," Vol. 3, March 1964, pp. 1–2; "No. 50 The System of Lunar Craters, Quadrant III," Vol. 4, May 1966, pp. 61–62; Arthur, D. W. G., Pellicori, R. H., and Wood, C. A., "No. 70 The System of Lunar Craters, Quadrant IV," *Communications of Lunar and Planetary Laboratory*, Vol. 5, May 1966, pp. 1.

[38] "Radar Studies of the Moon," Lincoln Lab. Report, April 1968, Massachusetts Institute of Technology

[39] Saari, J. M., "Lunar Thermal Anomalies and Internal Heating," *Astrophysics and Space Sciences*, Vol. 4, Jan. 1969, pp. 275–284.

[40] Middlehurst, B. et al., "Chronological Catalog of Reported Lunar Events," TR-277, Vol. 4, No. 63, July 1968, NASA.

[41] Watson, K., "I. Thermal Conductivity Measurements of Selected Silicate Powders in Vacuum from 150°−350°K; II: An Interpretation of the Moon's Eclipse and Lunation Cooling as Observed through the Earth's Atmosphere from 8-14 Microns," Ph.D. thesis, 1964, California Institute of Technology.

[42] Roelof, E. C., "Thermal Behavior of Rocks on the Lunar Surface," *Icarus*, Vol. 8, No. 1, Jan. 1968, pp. 138–159.

[43] Winter, D. F., "The Infrared Moon: Data, Interpretations, and Implications," Document D1-82-0900, Sept. 1969, Scientific Research Labs., The Boeing Co.

[44] Allen, D. A. and Ney, E. P., "Lunar Thermal Anomalies: Infrared Observations," *Science*, Vol. 164, April 1969, pp. 419–421.